Self-oscillations of an induced absorber (CdS) in a hybrid ring resonator

M. Wegener and C. Klingshirn
Physikalisches Institut der Universität Frankfurt, Robert-Mayer-Strasse 2-4, D-6000 Frankfurt am Main 1, Federal Republic of Germany
(Received 14 July 1986)

We investigate the properties of a material with excitation-induced increase of absorption in a hybrid ring resonator. The material is CdS at room temperature, showing photothermal optical nonlinearities. After characterizing the nonlinear medium itself, we investigate the behavior in a short Fabry-Perot resonator and then present experimental as well as theoretical data for this induced absorber in the ring cavity. We show experimental indications for the appearance of the Farey-tree structure, which was predicted theoretically in a recent paper. The dependence of the oscillations on various parameters is discussed.

INTRODUCTION

In recent years optical bistability (OB) gained a great interest, both from a fundamental point of view and from a more technical one. Many semiconductors were found to show strong optical nonlinearities under illumination with intense monochromatic laser light. These nonlinearities can have very different origins, e.g., the transition from excitons to biexcitons, the formation of an electron-hole plasma, or local heating of the sample. In CdS three types of OB—namely, OB due to induced absorption, due to saturable absorption, and dispersive OB—were clearly found using ns excitation in the $\mathrm{MW\,cm^{-2}}$ region. For recent reviews see, e.g., Refs. 1–5 and the literature cited therein. OB by saturable absorption was found at $T=300$ K. In contrast to these results much longer pulses (total length $\tau_L=100$ ms–10 s) lead to an increase of absorption for $\hbar\omega$ situated in the Urbach tail of the fundamental band gap. The mechanism is the heating of the sample resulting for CdS ($\mathbf{E}||\mathbf{c}$) and $\hbar\omega=2410$ eV (the green argon-laser line) in a sufficiently steep increase of the absorption as a function of temperature for the appearance of intrinsic OB by induced absorption.[2,3,6] This nonlinearity will be the interesting one in the following. Recently, self-oscillations were theoretically predicted by Ref. 7 for an induced absorber in a ring cavity. Both theory[8] and experiments[9] have been done so far for a ring cavity containing a medium exhibiting mainly dispersive nonlinearities (Kerr medium). This system leads to oscillatory instabilities and ways to chaos. As will be shown, the structure of the oscillations is totally different for an induced absorber which, in contrast to dispersive nonlinear media, may be intrinsically bistable. The motivation to do our experiment is twofold:

(i) Our system allows us to study nonlinear dynamics whereby both the nonlinearity and the feedback can be controlled separately.

(ii) Although we use a hybrid feedback leading to a loss of phase, our results are applicable to the all-optical system, which will be discussed in Sec. III. This system might be a candidate for an all-optical clock in connection with all-optical computing.

In the following sections we will show

(a) the intrinsic properties of the induced absorber CdS,

(b) its behavior in a short Fabry-Perot (FP) resonator,

(c) the experimental setup, and

(d) the static properties of the medium in a ring cavity, leading to the first direct measurement of the third unstable branch of the intrinsic bistability.

(e) We then present the self-oscillations.

We shall discuss the dependence of the oscillations on the different parameters showing, among others, experimental indications for the Farey-tree structure predicted by Ref. 7(c).

I. THE BEHAVIOR OF THE NONLINEARITY WITHOUT ADDITIONAL FEEDBACK

It is a well-known fact that the optical properties of semiconductors depend on the temperature T of the sample. Many insulators and semiconductors show an absorption edge, which can be described by the Urbach-Martienssen rule[10]

$$\alpha(\omega,T)=\alpha_0\exp[\sigma(\hbar\omega-E_0)/k_BT]\ , \tag{1}$$

where σ and α_0 are material parameters, E_0 corresponds roughly to the energy of the lowest free exciton, and k_B is Boltzmann's constant. At photon energies $\hbar\omega$ below the fundamental band edge an increase of the sample temperature results in an increase of the absorption α. A small laser spot increases the local temperature T by the absorption of photons which generate primarily electron-hole (e-h) pairs. This excitation finally thermalizes. Because the lifetime of e-h pairs is of the order of 1 ns, this intermediate step can be eliminated adiabatically. The temporal evolution of $\Delta T=T-T_0$ (with T_0 being the temperature of the surrounding heat bath) can be modeled by Eq. (2):

$$\frac{d}{dt}(\Delta T)=-\Delta T/\tau+A(\Delta T)I(t)/(CL) \tag{2}$$

with

$$A(\Delta T)=1-\exp[-\alpha(\Delta T)L] ,$$

$$I_t(t)=I(t)\exp[-\alpha(\Delta T)L] .$$

The first term on the right-hand side describes the diffusion of the excitation in the lateral direction resulting in a relaxation time constant τ for the local temperature increase. τ depends on the diameter of the spot d, with $\tau\sim d^{-2}$. For $d=100$ μm one obtains the estimate[6] $\tau=150$ μs, which will be used in the following. The second term describes the excitation depending on the absorbed fraction $A(\Delta T)$ of I, I being the intensity in front of the crystal which obviously coincides with the incident intensity I_0 if no cavity is present. $A(\Delta T)$ is obtained by averaging the intensity inside the crystal over the length L of the sample. This is allowed as long as the diffusion of electronic and thermal excitation is sufficiently large for a homogeneous excitation in the depth of the sample. The CdS crystals are of the platelet type, with the crystallographic **c** axes being in the plane of the platelet. Here we have used samples with a thickness between 3 and 10 μm, the polarization is always $\mathbf{E}||\mathbf{c}$. Figure 1 shows the measured $A(\Delta T)$ (Ref. 6) for a CdS single-crystal platelet, $\mathbf{E}||\mathbf{c}$. If ΔT is also eliminated adiabatically, one may use the well-known graphical construction[11] to solve Eq. (2). This results in three mathematical solutions out of which two are physically stable, as can be shown by stability analysis. Therefore there is a region of I_0 where two transmitted intensities I_t are possible for one incident intensity I_0, depending on the way to I_0. An observer will not get any direct information about this third unstable branch. Figure 2 shows the resulting hysteresis with the switching times being $\tau_\downarrow\approx 2$ ms and $\tau_\uparrow\approx 5$ ms. If the total length τ_L of the pulses is decreased, one can see a dynamical overshooting of the switching intensities caused by a mismatch between ΔT and the incident intensity I_0. For a detailed discussion of these effects see Ref. 6, where the behavior of the rate Eq. (2) is shown to be in good agreement with the experimental results. In Ref. 6 also the setup is shown, which uses a cw argon-ion laser. The pulses are generated with an electro-optic modulator. Both incoming and transmitted intensities are detected by photodiodes. In this context it is important to remark that the switching time is no intrinsic constant for the system but depends strongly on the way to the critical switching temperature. This leads to the critical slowing down, well known, e.g., for dispersive OB.[12] We look at the situation, where one switches on a constant I_0 at time $t=0$, being slightly above the switching-down intensity $I_\downarrow$. The time until the onset of switching τ_1 and the time necessary for the switching process τ_2 will diverge for $I_0-I_\downarrow\to+0$. To describe the situation one can roughly approximate $A(\Delta T)$ (Fig. 1) by three straight lines (also see Ref. 7) leading to analytic expressions for τ_1 and τ_2 as a function of $\delta=(I_0-I_\downarrow)/I_\downarrow$ by solving Eq. (2) with $\Delta T(\tau_1)=\Delta T_1$ and $\Delta T(\tau_1+\tau_2)=\Delta T_2$, $\Delta T(0)=0$:

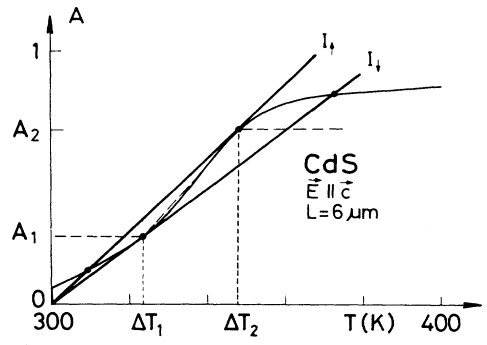

FIG. 1. Measured $A(\Delta T)$ for a 6-μm CdS crystal. The straight lines show that OB is expected to appear. $\hbar\omega=2410$ eV (according to Ref. 6).

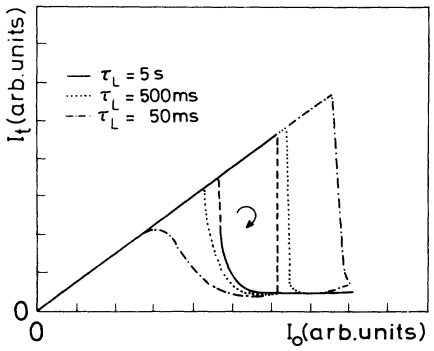

FIG. 2. Experimental observation of OB by induced absorption using CdS at $T=300$ K. Note the increase of dynamic effects for decreasing pulse duration τ_L; $\hbar\omega=2410$ eV.

$$\tau_1/\tau=\ln[(1+\delta)/\delta] ,$$
$$\tau_2/\tau=\left[\frac{\Delta T_1}{A_1}\frac{A_2-A_1}{\Delta T_2-\Delta T_1}(1+\delta)-1\right]^{-1} \times\ln\left[\left[\frac{A_2}{A_1}(1+\delta)-\frac{\Delta T_2}{\Delta T_1}\right]\Big/\delta\right] . \quad (3)$$

Choosing $A_1=0.27$, $A_2=0.69$, $\Delta T_2=2\Delta T_1$, which fits to Fig. 1, we obtain $\tau_1\approx 4.6\tau$ and $\tau_2\approx 7.1\tau$ for $\delta=1\%$. Obviously τ_1 and τ_2 are of the same magnitude. Note that Eq. (3) only makes sense for an intrinsically bistable system, i.e., $\Delta T_2/\Delta T_1<A_2/A_1$.

Figure 3 shows what we have observed when switching on constant $I_0=(1+\delta)I_\downarrow$ in the beginning and detecting I_t as a function of time. For $\delta=0$ one observes a more or less exponential decrease of I_t until a constant level is reached. This decrease results from the increase of absorption at temperatures which are smaller than the critical switching temperature. This effect is very pronounced because the series is taken with a $L=9$ μm crystal, which is quite thick. With increasing δ we again obtain the first decrease, but after a certain time delay τ_1 the absorptive switching process starts and a constant low transmitting level is reached after a few ms, which on this time scale leads to an almost perpendicular transition. The time delay τ_1 decreases with increasing I_0 or δ. In this case more

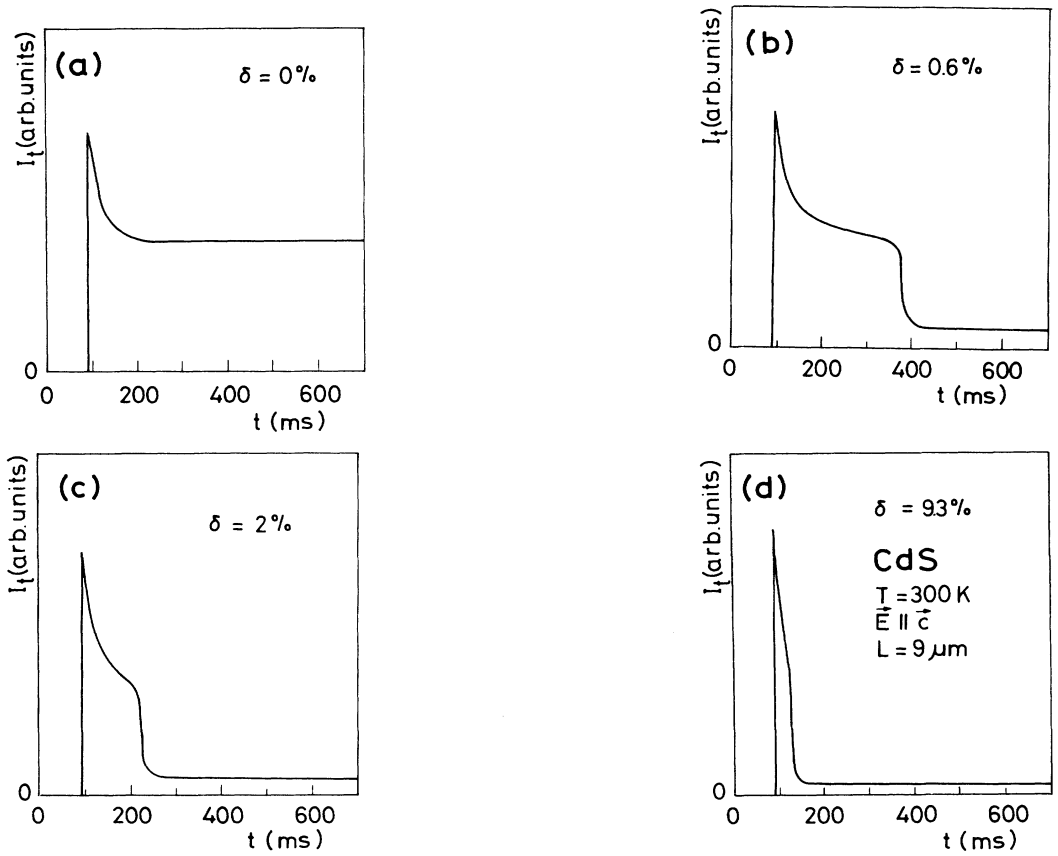

FIG. 3. Experimental results for the critical slowing down. The constant incident intensity I_0 is switched on at $t \approx 90$ ms; $\hbar\omega = 2410$ eV.

and more energy is pumped into the system, which leads to a faster heating of the spot and therefore a shorter τ_1. Figure 4 now shows τ_1 as a function of δ, showing within experimental limitations the divergence of τ_1 for $\delta \to 0$. The pole structure may be destroyed by the existence of a small noise level which leads to a finite value of τ_1 for $\delta = 0$. Comparing experiment and theory one finds that τ_2 fits well (theory, $\delta = 1\% \to \tau_2 \approx 1.1$ ms; experiment; few ms), but τ_1 is distinctly longer in the experiments.

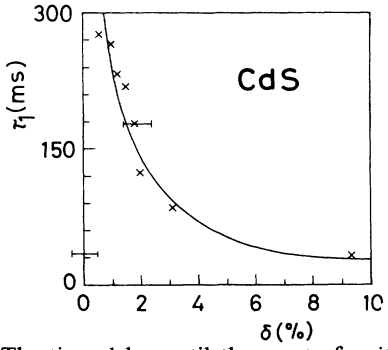

FIG. 4. The time delay until the onset of switching τ_1 as a function of δ, gained from a series of measurements like the ones in Fig. 3; $\hbar\omega = 2410$ eV.

II. THE NONLINEARITY IN CONNECTION WITH THE FEEDBACK OF A SHORT EXTERNAL FABRY-PEROT CAVITY

As described, the OB by induced absorption is an intrinsic mechanism, needing no additional external feedback. But what is going on if we add a feedback of the light field by using an external FP? Looking at the situation where we start in the transmission maximum of the FP mode structure, an increase of absorption will lead to a decrease of the finesse of the FP. This results in a smaller generation rate of ΔT because the intensity inside the FP is reduced. But the intrinsic absorptive switching to the highly absorbing state was connected with an increase of $\alpha(\Delta T)$. So the FP leads to a negative feedback which might destroy the bistability if the intrinsic positive feedback cannot overcompensate the negative feedback of the cavity. But now in connection with the external FP, dispersive nonlinearities also become relevant, which are always connected with the absorptive nonlinearities via Kramers-Kronig relations. These two influences may lead to very complicated hysteresis loops.

In our experiment we have coated the CdS platelets with dielectric mirrors on both sides each with reflectivity $R \approx 60\%$. The effect of these coatings on the mode struc-

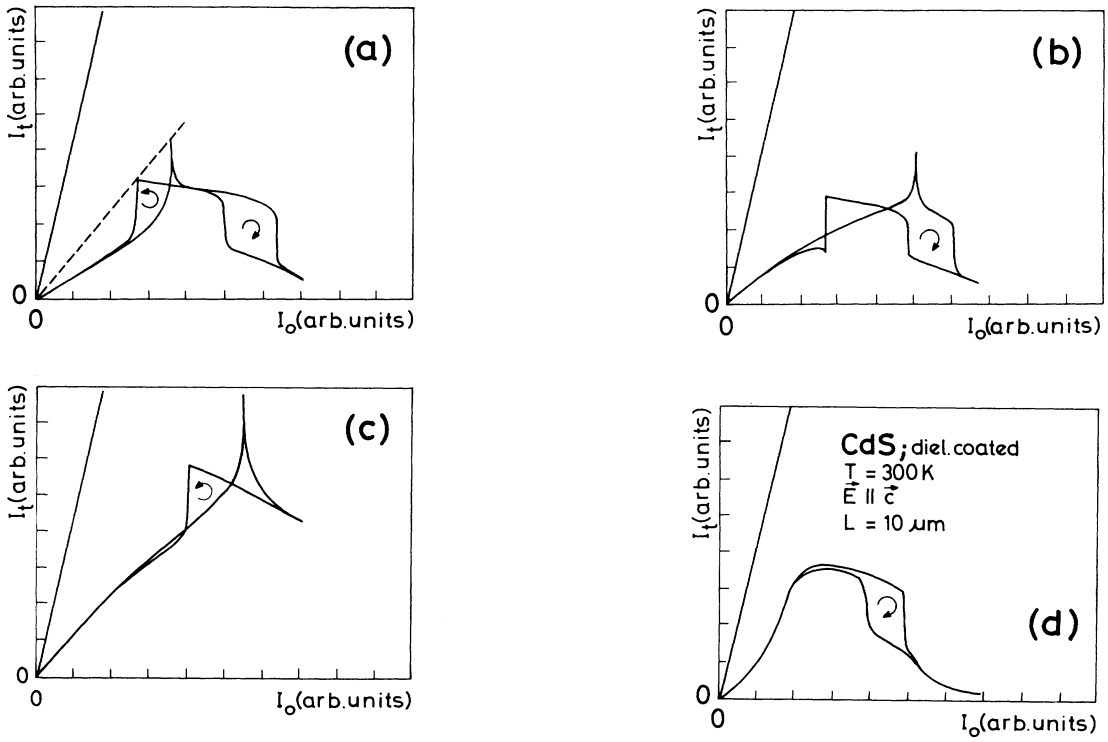

FIG. 5. A series of measured hysteresis loops $I_t(I_0)$ for dielectric-coated CdS platelets, changing only the place on the crystal resulting in small changes of R and δ_0; $\hbar\omega = 2410$ eV.

ture is a bit reduced by imperfections of the surfaces. Figure 5 shows the result of a series of measurements. Obviously one can obtain very different loops, strongly depending on the initial phase δ_0 inside the FP. Changes of the sample's thickness in the order of parts of the wavelength might shift the mode structure from a maximum to a minimum.

In Fig. 5(a) the situation is relatively simple. We first obtain a purely dispersive switch up in the transmitted intensity connected with a transient spike resulting from the shift over the FP maximum. For twice the incident intensity, an absorptive switch down occurs. Dispersive and absorptive loops are clearly separated. But note that the area enclosed by the absorptive loop has diminished, in comparison with Fig. 2, caused by the negative feedback of the FP. In Fig. 5(b) we start close to a maximum of the FP mode structure. This situation manifests itself in the overshooting at the dispersive switch back (↓). Here dispersive and absorptive loops are no longer separated. This trend is continued in Fig. 5(c), where the dispersive switch up (again connected with the overshooting) more or less coincides with the absorptive switch down.

To get some more insight, we again use Eq. (2) combining it with the usual resonator formula for the FP:

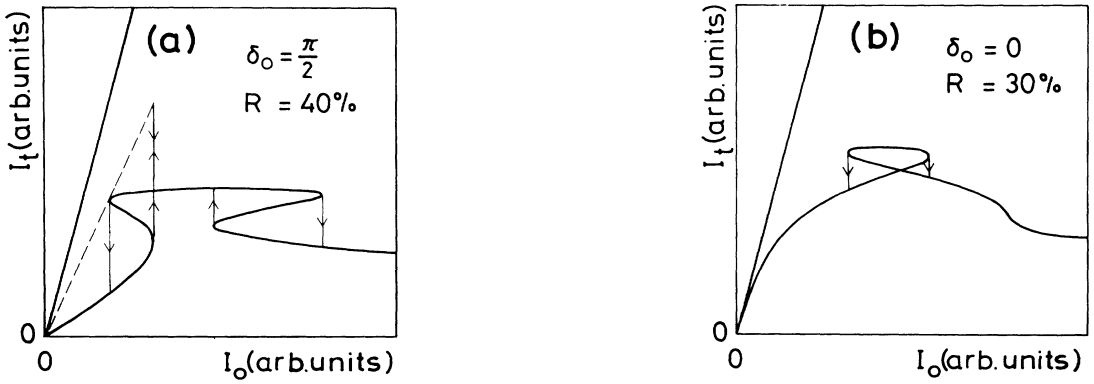

FIG. 6. Theoretical mixed states of dispersive and absorptive OB using Eq. (3) in the steady-state limit. Note that between (a) and (b) mainly the initial phase δ_0 is changed leading to totally different hysteresis loops; $\hbar\omega = 2410$ eV.

$$\frac{d}{dt}(\Delta T)=-\Delta T/\tau+\alpha(\Delta T)(1-R)(1+R)I_0(t)/C\{[\exp(\alpha L/2)-R\exp(-\alpha L/2)]^2+4R\sin^2(\delta_1)\}\ ,$$

$$\delta_1=\delta_0+k_0L\times\text{const}\times\Delta T\ , \tag{4}$$

$$I_t=I_0(1-R)^2/\{[\exp(\alpha L/2)-R\exp(-\alpha L/2)]^2+4R\sin^2(\delta_1)\}\ .$$

For simplicity we assume that the refractive index changes linearly with temperature. Solving Eq. (4) in the adiabatic limit [$d(\Delta T)/dt=0$], we obtain Fig. 6. In Fig. 6(a) we start in a FP minimum ($\delta_0=\pi/2$), obtaining a hysteresis which looks very much like Fig. 5(a). Figure 6(b) shows again the more involved situation where dispersive and absorptive switchings cannot be separated leading to a butterflylike hysteresis which is qualitatively the same as Fig. 5(c) ($\delta_0=0$ corresponds to the FP maximum).

In the beginning of this section we discussed the negative feedback of the FP. Why does this mechanism not lead to self-oscillations? It does not, because the time constant for filling the FP with light (order of ps) is small compared to the system time constant τ and therefore a fixed point is always reached. But if the delay of the external feedback is long enough, the stable solutions shown in Sec. IV will change to oscillatory output, as will be shown in Sec. V.

III. THE INDUCED ABSORBER IN A RING CAVITY: EXPERIMENTAL SETUP

The system we are dealing with is shown in Fig. 7(a). The light transmitted by the sample is reflected by the mirrors and therefore coupled back with the delay of one round-trip time τ_R. In this system one has to add field amplitudes and to take into account also dispersive changes, provided the coherence time of the light source is larger than τ_R. The dispersive effects are not that important for the oscillations as shown in Refs. 7(a) and 7(b), where calculations with and without taking into account dispersive effects are directly compared, showing no important difference. In Fig. 7(b) we present the hybrid system, which we use in our experiment. In this system we lose information about phase, which would be the same in case of the coherence length of the laser being smaller than the length of the cavity.

We send in a beam of constant intensity from a linearly polarized cw argon laser into the electro-optic modulator (EOM), which consists of a Pockels cell in connection with a polarizer. To avoid a Gaussian profile of the laser spot on the sample, we select the central part by a diaphragm before focusing the laser on the crystal. The homogeneous spot has a diameter of 100 μm. The transmitted beam is then sent on the photodiode after passing some neutral density filters. The voltage signal is digitized with a resolution of 8 bit and a maximum sampling rate of 1 MHz. The digitized signal is stored in a few kbyte of random access memory (RAM) for a maximum of 2000 sampling times. The delay time therefore results from the product of sampling time and storing cycles. Both are variable, but we usually keep the storing cycles constant at 1000 and vary the sampling rate. This means we have always digitized 1000 points in one round-trip time τ_R. After a digital-to-analog conversion we can attenuate the signal (corresponding to variable R of the mirrors) and add an additional offset (standing for the constant input I_0) before the signal is connected with the Pockels cell via a high-voltage amplifier. There is a certain nonlinearity in the feedback system, coming from the Pockels cell, which causes the quadratic increase in the following $I_t(I)$ or $I_t(I_0)$ pictures for small values of I before the linear regime is reached. Therefore the scales of I_0 between experiment and theory can only be compared qualitatively. R^2 (see Sec. V) is defined experimentally by normalizing the transmission in the highly transmitting state to be equal to one.

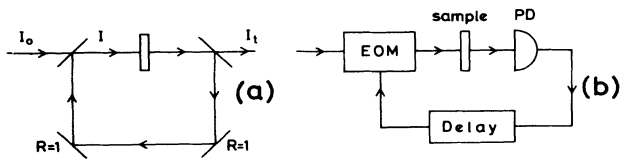

FIG. 7. (a) Induced absorber in a ring cavity; (b) schematic representation of the hybrid system used in our experiment.

IV. THE CASE OF SMALL τ_R ($\tau_R \ll \tau$)

To describe the properties of the cavity we use the delay equation

$$I(t)=I_0+R^2I_t(t-\tau_R)$$
$$=I_0+R^2I(t-\tau_R)\exp[-\alpha(\Delta T(t-\tau_R))L]\ . \tag{5}$$

Thereby I_0 denotes the incident intensity, counted behind the first mirror, which is easy to handle and corresponds to what we can measure directly in our system. The dynamics of the temperature is again described by Eq. (2).

This coupled delay and rate equations have also been used in Ref. 7, except that we add intensities instead of field amplitudes and more important we do not use the simplified nonlinearity $A(\Delta T)$, using three straight lines (see Sec. I), but take a fit to the real measured dependence $A(\Delta T)$ for our calculations (see Fig. 1). The case of $\tau_R \ll \tau$ has not been interpreted in Ref. 7(a) in the way done here. The case of $\tau_R \gg \tau$, which will be discussed in Sec. V, and the dependence of the oscillations on τ_R (see Sec. VI) reveals quite similar results although totally different $A(\Delta T)$ are used, showing that the details of $A(\Delta T)$

are not very important as long as the induced absorber is intrinsically bistable. We want to discuss this situation only in the present paper.

Looking at $\tau_R \ll \tau$ again, no oscillations will appear, i.e., $I(t)=I(t')\ \forall t,t'$. The situation is very similar to the short FP, starting in a FP maximum. Again a sufficient reflectivity will destroy the intrinsic absorptive bistability, i.e., $I_t(I_0)$ is not bistable any more. But what we are going to look at is $I_t(I)$ [not $I_t(I_0)$]. This point is the important new one. It is the situation of an observer looking from the crystal's point of view of what is going on. He now is no longer able to vary I at his own will, but is only observing what a certain I_0 causes for I and I_t. Figure 8 shows what we have observed for increasing "reflectivity R" of the mirrors. $I_0(t)$ is a triangular pulse of total length $\tau_L=10$ s to be free from any dynamic effects.

For $R^2=0\%$ the normal intrinsic bistability is obtained (the quadratic increase is explained in the previous section). For $R^2=25\%$ something strange happens. The switching processes have now a steep positive slope (dashed lines) until at $R^2=50\%$ there is only a small unstable region vanishing completely for $R^2=75\%$. Here we have three stable solutions for I_t as a function of I. We interpret this third branch as the third normally unstable branch of the intrinsic bistability.

To confirm this interpretation theoretically, we use Eq. (2) together with Eq. (5) [$d(\Delta T)/dt=0$]. If we are interested in $I_t(I)$ (what we have measured), we only need Eq. (2). Note that one yields $I(\Delta T)$ and $I_t(\Delta T)$, leading to the S-shaped dependence $I_t(I)$ in Fig. 9, independently of the reflectivity R. [R does not appear in Eq. (2).] Only the range of stable solutions will depend on R. In order to obtain this range we get $I_0(\Delta T)$ and $I_t(\Delta T)$ from Eq. (2) and Eq. (5) which introduces the dependence on R leading to $I_t(I_0)$ as is also shown in Fig. 9. The stability range for $I_t(I_0)$ can easily be gained. The switching processes are perpendicular as is known from OB itself, where always I_t as a function of I_0 is presented. The beginning and end of the graphically obtained transitions in $I_t(I_0)$ can be transferred by horizontal lines to the $I_t(I)$ curve. So we obtain for $R^2=25\%$ a hysteresis similar to the measured one in Fig. 8(b) ($R^2=25\%$).

If $I_t(I_0)$ is not bistable any more [as is the case in Fig. 8(d) ($R^2=75\%$)], every point on $I_t(I)$ becomes stable. Because the $I_t(I)$ curve does not depend on R (but only its stability range does) this curve is identical with the $I_t(I_0)$ curve for $R^2=0\%$ (where $I=I_0$), which is the intrinsic bistability (including the unstable branch) of the medium.

This theoretical background finally allows us to identify the measured third branch with the third normally unstable branch of the intrinsic bistability of the medium.

V. THE CASE OF LONG τ_R ($\tau_R \gg \tau$)

If $\tau_R \gg \tau$, many solutions from the case $\tau_R \ll \tau$ (where I_t always was constant) become unstable leading to oscil-

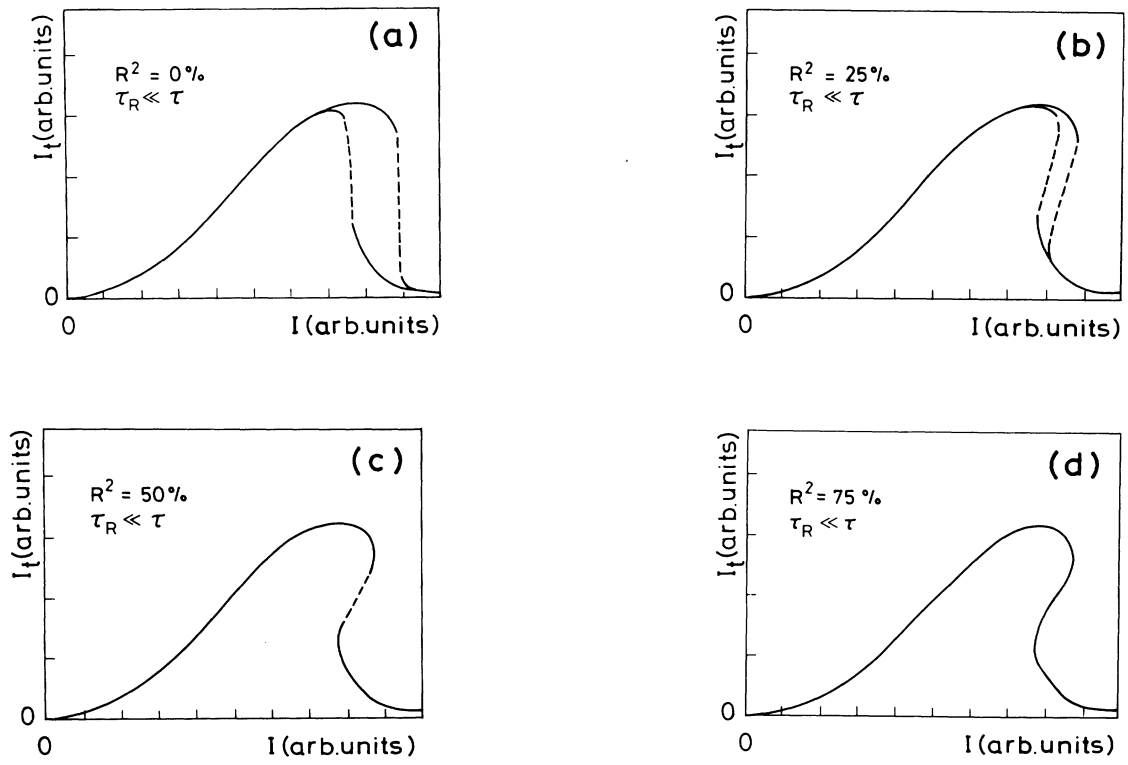

FIG. 8. I_t as a function of I (not I_0) for increasing reflectivity R of the mirrors. Note the diagonal switching for $R^2=25\%$ and $R^2=50\%$.

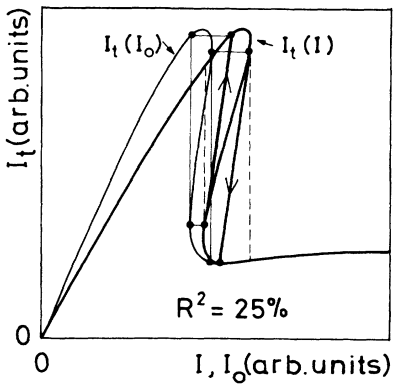

FIG. 9. Graphical construction to obtain the diagonal transitions for $I_t(I)$.

latory output of the cavity at constant I_0. The basic mechanism for all oscillations is the retarded negative feedback by the cavity. This negative feedback may be revealed by two different mechanisms.

The first one is the decrease of I if the switching down to low transmission occurs. Starting with $I<I_\uparrow$ the intensity I will increase n times every round trip by a certain amount until $I>I_\downarrow$. Now the medium switches to the low transmitting state causing I to decrease m times until $I<I_\uparrow$. In the following we will denote such an oscillation as an (n,m) mode in agreement with Ref. 7(a).

The second mechanism is the negative slope of $I_t(I_0)$, when decreasing I_0 towards $I_\uparrow$ being on the lower branch of the hysteresis [see Fig. 2 or Fig. 8(a)]. If I increases, I_t decreases, decreasing I, which increases I_t, increasing I back to the initial value. Under the present conditions only oscillations of period two may occur. We denote this type as an $(\underline{1,1})$ mode to distinguish it from the $(n=1,m=1)$ mode of the first mechanism, which we now call $(\overline{1,1})$. This second mechanism has not been discussed in Ref. 7(a). We will leave out the overbar for all $(n\neq 1,1)$ modes, because no confusion is possible.

In the following we will discuss both mechanisms experimentally as well as theoretically. Figure 10 shows a measured series of oscillations using I_0 as a control parameter. For $I_0=68.5\%I_\downarrow$ and $R^2=75\%$ we observe an oscillation which is called a (2,1) mode (twice up, once down) in our terminology, showing spiking at the beginning and end of every step. To understand the spikes imagine the situation where we switch on I_0 resulting in steps without spikes until $I>I_\downarrow$. Although we are in the limit $\tau_R \gg \tau$, the medium will need a certain time to react to this new situation, due to the relaxation dynamics of the temperature. During this time also, I_t will rise until the onset of switching to low transmission. After one

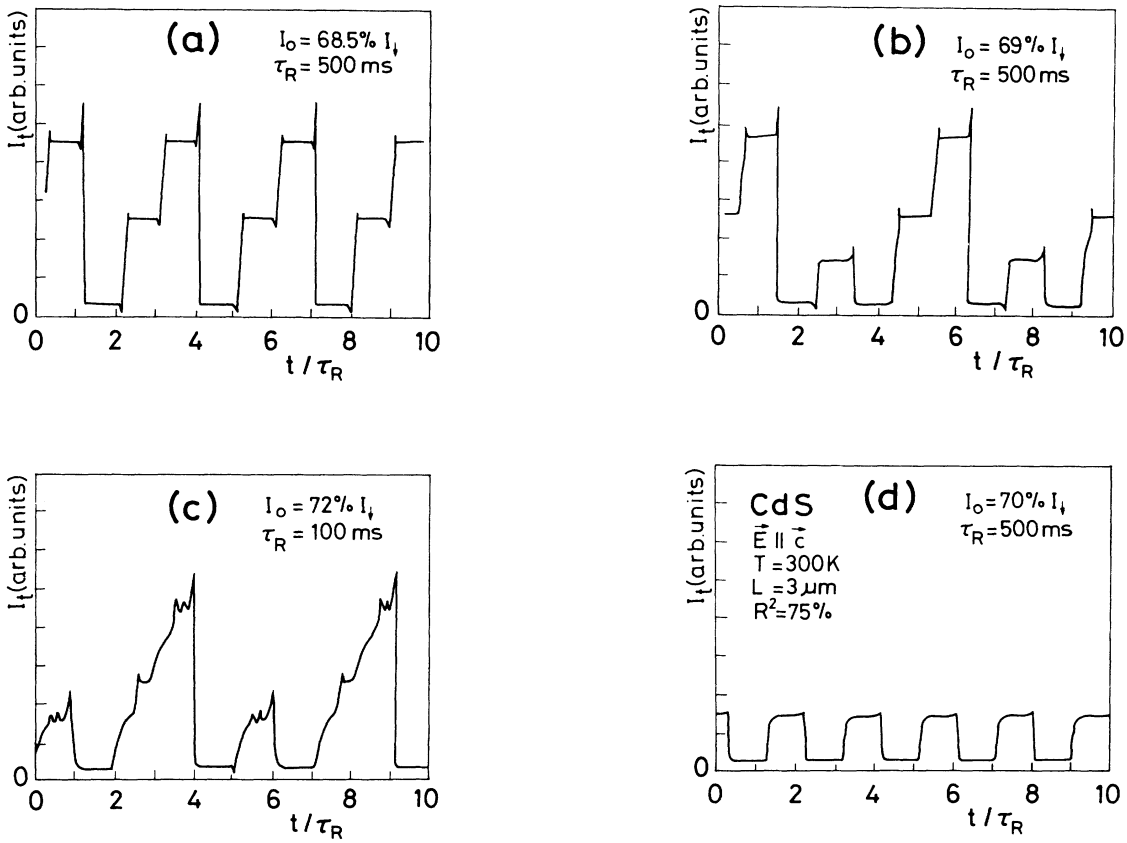

FIG. 10. Series of measured $I_t(t)$ curves showing a Farey-tree-like structure with I_0 being the control parameter.

round-trip time this spike arrives in front of the crystal causing a new one at the end of the next step in the oscillation. After a short transient phase the oscillations become periodic together with the spiking structure. For $I_0 = 70\% I_\downarrow$, the ($\underline{1,1}$) mode, due to the second mechanism, is observed. I_t is smaller compared to the (2,1) mode because the crystal remains on the low transmitting branch of the intrinsic bistability.

The question is what is happening if I_0 is chosen in between the (2,1) and ($\underline{1,1}$) modes. We find an oscillation [Fig. 10(b)] which alternates periodically between the two ones. It has a period of about $5\tau_R$ and an average period of $\frac{5}{2}\tau_R$, respectively. While the simple (2,1) or ($\underline{1,1}$) modes are stable for many hours, the alternating one is observed to be stable a maximum of about 2 min, before the system decided to oscillate in one of the simple types. Looking in more detail at the alternating mode in Fig. 10(b), one can see a little shoulder, which becomes much more pronounced in Fig. 10(c) (τ_R is decreased to 100 ms). This shoulder results from the critical slowing down at the point of switching back to the highly transmitting state. If τ_R is further decreased, this alternating mode vanishes.

In order to get a better understanding of the nature of the alternating mode and of the structure of the modes as a function of I_0, we theoretically investigate the limit $\tau_R \gg \tau$ following the idea of Ref. 7(c). We transform Eq. (5) together with Eq. (2) to a simple map

$$I_{n+1} = I_0 + R^2 I_t(I_n) \; . \tag{6}$$

Looking at Fig. 10(a) that means neglecting the spikes on the steplike oscillations. To simplify the situation further we use the dependence $I_t(I_0)$ as shown in the small picture in Fig. 11 which schematically describes our findings. By simply iterating Eq. (6), we obtain the whole period T of the oscillations in multiples of τ_R as a function of I_0, as shown in Fig. 11(a). Between the simple (n,1) modes

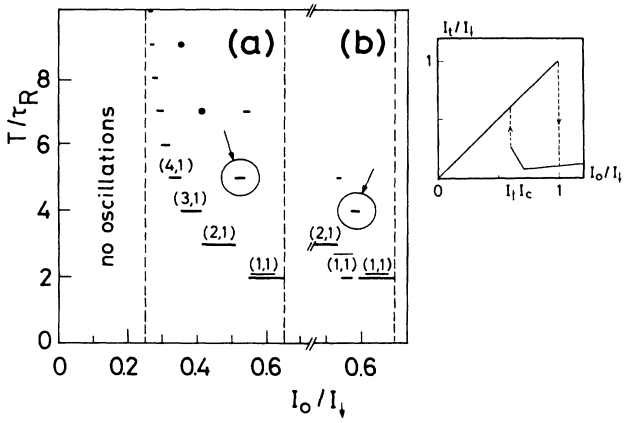

FIG. 11. (a) T/τ_R as a function of $I_0/I_\downarrow$ as calculated by iterating Eq. (6) with $I_t(I_0)$ as shown in the small plot; (b) with 5% reduced width of the hysteresis loop.

are trees of longer periods, whereby twice only the first step of the tree is visible on this scale. These trees are generic for the transition between modes of different frequencies in this system as shown in Ref. 7(c). They exhibit a Farey tree structure.

We again choose the example of the tree between the (2,1) and ($\underline{1,1}$) modes, also discussed in the experimental part.

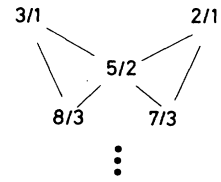

(7)

In Eq. (7) we denote the average period of the oscillations as p/q whereby p is the total period T and q is the number of different maxima. Starting with 3/1 [corresponding to the (2,1) mode] and 2/1 [corresponding to the ($\underline{1,1}$) mode], one has to add numerators and denumerators independently resulting in 5/2 in the second generation. The following generations can be obtained in the same manner. The more maxima an oscillation has, the smaller is its stability range. This coincides very well with our experimental findings. If the noise level of the system becomes comparable with the stability range, the mode will not be observed.

Another example of such a tree is given in Fig. 12 and Fig. 11(b). In Fig. 12 we have chosen a place on the crystal with greater thickness L, leading to a decrease of the intrinsic bistable regime of the medium. (Also see Ref. 6 for a detailed discussion of the dependence of the bistability on L.) Again we only observe the first step of the tree being an oscillation alternating periodically between ($\overline{1,1}$) and ($\underline{1,1}$) modes. We have modeled this situation in Fig. 11(b) theoretically by iterating Eq. (6) with $I_t(I_0)$ analogue to the small picture in Fig. 11 but with a width of the hysteresis reduced by 5%.

If I_0 is too high, i.e., a fixed point on the lower branch of the bistability exists, a damped oscillation is observed in experiment as well as theoretically when solving Eq. (5) combined with Eq. (2) numerically. Figure 13(a) shows such a damped oscillation, switching on I_0 between $t = 4\tau_R$ and $t = 5\tau_R$ resulting in an exponential-like decrease before one round-trip time later the medium switches to low transmission leading to a fixed point after $t \approx 20\tau_R$. Figure 13(b) coincides with Fig. 13(a) except that the absolute time constants do not fit well. The calculation was done for $\tau_R = 10\tau = 1.5$ ms and corresponds to the experimental $\tau_R = 100$ ms, showing the same mismatch as discussed in the beginning when talking about critical slowing down.

To get an overview where the plateaus of the steplike oscillations are situated as a function of I_0, we are now looking at $I_t(I_0)$ which is multivalued in the limit $\tau_R \gg \tau$. Experimentally we use a very small sweep frequency

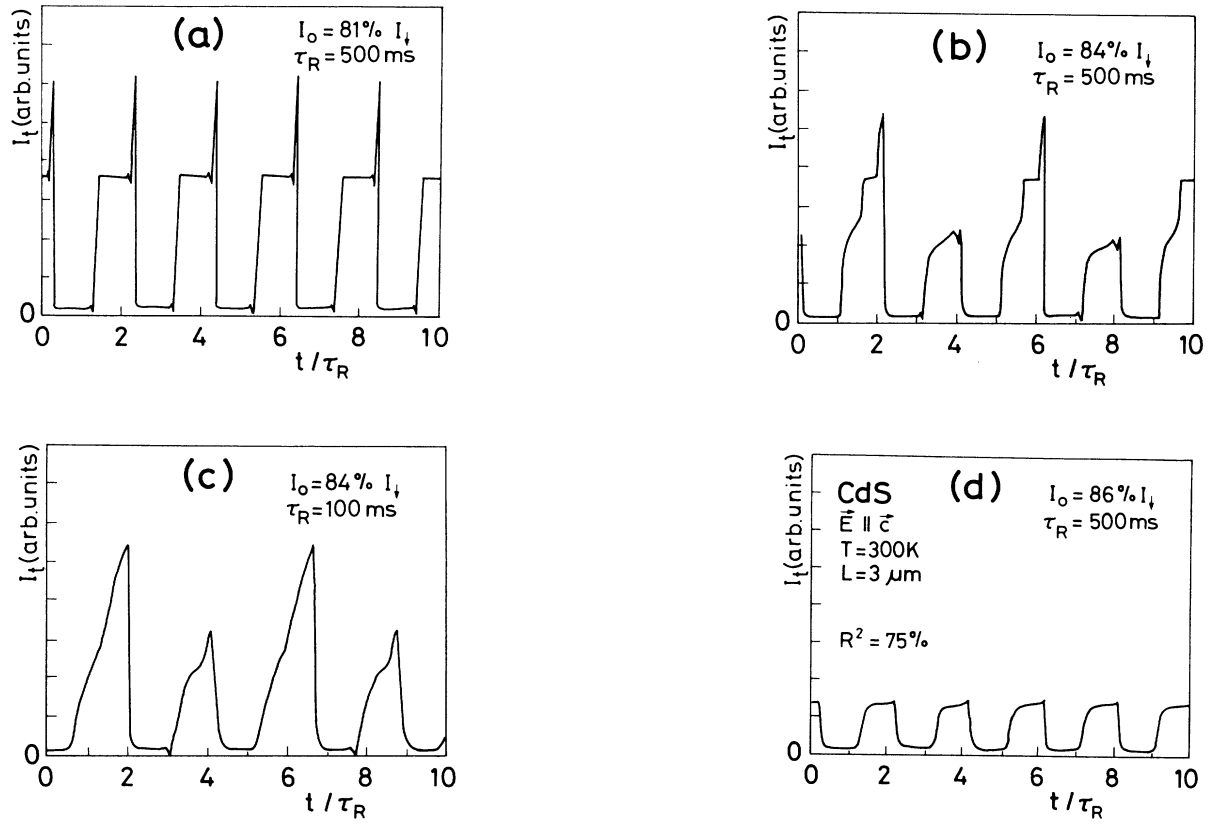

FIG. 12. Series like Fig. 10, but with a smaller intrinsically bistable hysteresis.

$f \ll \tau_R^{-1}$ to scan I_0 and connect this with the x axes of an oscilloscope, I_t (the photodiode signal) with the y axes of a scope. This procedure results in Fig. 14(a). For small I_0 only one stable branch exists because the losses ($R^2 = 75\%$) are too high to increase I beyond $I_\downarrow$. These fixed points are situated on the highly transmitting branch of the hysteresis. At a critical value oscillations are appearing having long periods, the longest observed was a (20,1) mode. In principal (∞,1) modes should exist here. For increasing I_0 the plateaus (corresponding to the white zones) also increase up to a certain value where the highest one leads to $I > I_\downarrow$ which is just the transition from a ($n+1$,1) to a (n,1) mode. For high I_0 again the (1,1) mode exists before I_0 is too large for oscillations, corresponding to Fig. 13. The same behavior is found theoretically [Fig. 14(b)] by again iterating Eq. (6) with

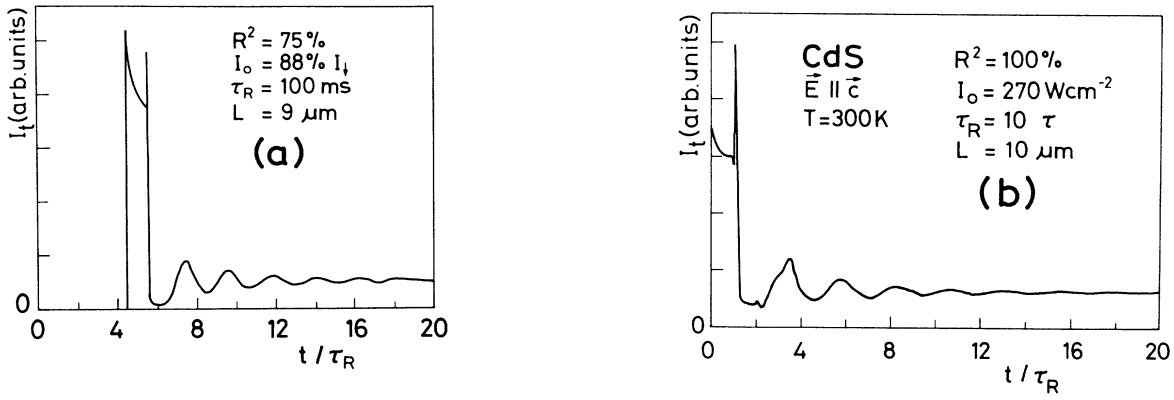

FIG. 13. (a) Damped oscillation as observed for I_0 being beyond the oscillatory regime; (b) same situation but calculated numerically with Eqs. (2) and (5).

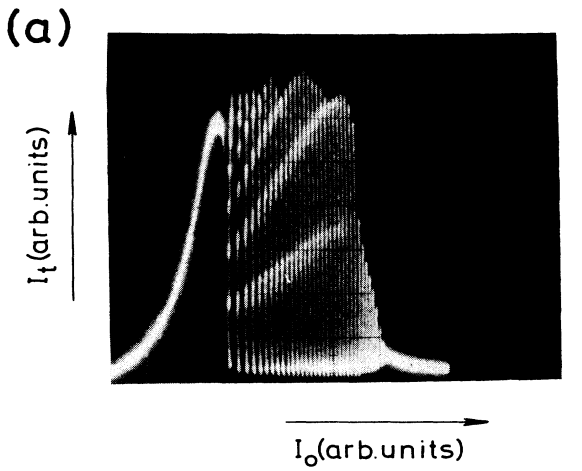

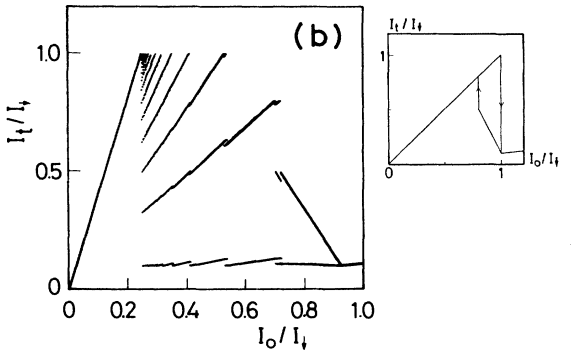

FIG. 14. (a) Experimental $I_t(I_0)$ curves using a slow ramp to increase I_0, $\tau_R=100$ ms, $R^2=75\%$, $\mathbf{E}\|\mathbf{C}$, $T=300$ K, $L=9$ μm; (b) theoretical $I_t(I_0)$ curve gained from Eq. (5) and $I_t(I)$ describing the hysteresis of a 9-μm CdS crystal as shown in the small plot.

$I_t(I)$ as shown in the small picture in Fig. 14, which roughly describes the findings for a $L=9$-μm-thick CdS platelet. Note that the fine structure in Fig. 14(b) and the Farey tree are not resolved in Fig. 14(a) because of the finite sweeping frequency.

VI. THE DEPENDENCE OF THE OSCILLATIONS ON τ_R

Figure 15 shows a series of oscillations with decreasing τ_R. Starting with $\tau_R=500$ ms ($\gg\tau$), a (2,1) mode is obtained which has not as many spikes as the one for a $L=3$-μm-thick crystal because at $L=9$ μm, $A(\Delta T)$ (see Fig. 1) is rounded very much (see also Fig. 8). The total period T of this oscillation is slightly above $3\tau_R$. Keeping I_0 constant and only varying τ_R, Fig. 15 shows for $\tau_R=50$ ms an oscillation which has lost some of the steplike structure and is no longer locked into $T=3\tau_R$, but T is approximately $4.7\tau_R$. This tendency continues for $\tau_R=5$ ms where $T\approx 8.9\tau_R$ leading to an almost sinusoidal oscillation. Decreasing τ_R further stops oscillatory output at $\tau_R\approx 2$ ms. For small τ_R obviously τ is the dominating time constant and no longer τ_R, leading to the disappearance of locking of T into multiples of τ_R. The corresponding Poincaré-like plot is always shown on the right-hand side. Although we display $I_t(t)$ versus $I(t)$, Eq. (5) shows that $I_t(t)=R^{-2}[I(t+\tau_R)-I_0]$ means that only the ordinate is rescaled. For $\tau_R=500$ ms the dots correspond to the plateaus in the oscillations. This loop is also drawn in the Poincaré section for $\tau_R=50$ ms and $\tau_R=5$ ms to be easily compared. The effect for $\tau_R=5$ ms is very drastic. Neither the high nor the low transmitting branch are reached; a transmission in between is always obtained. To have a direct comparison to our model we again solve Eq. (2) with Eq. (5) numerically. The general

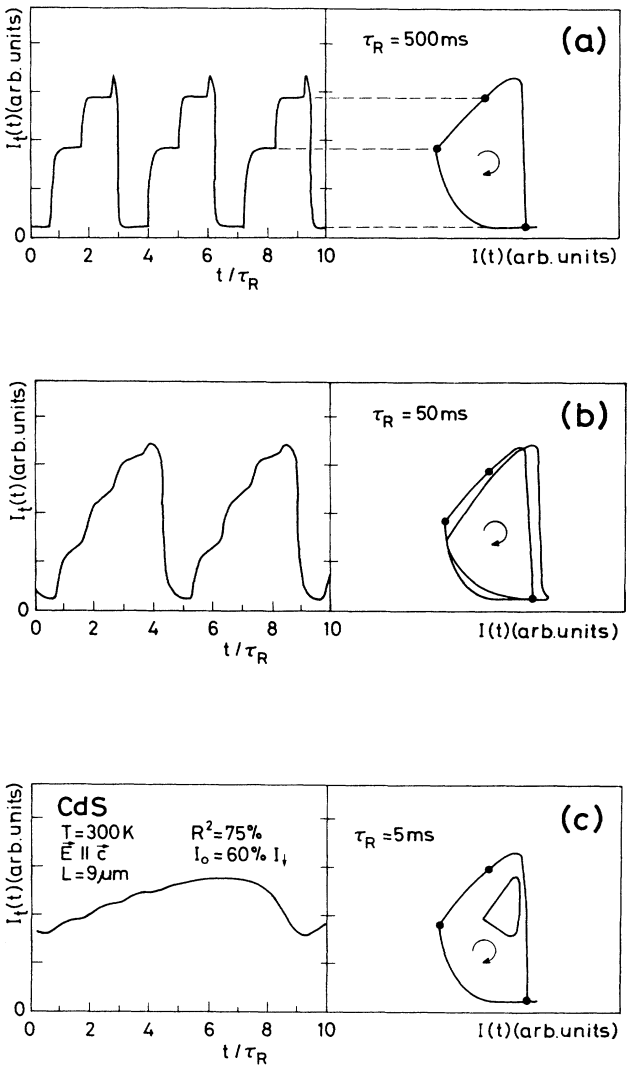

FIG. 15. Experimental series of $I_t(t)$ curves keeping I_0 constant and decreasing τ_R starting with $\tau_R\gg\tau$. The picture on the right-hand side always shows the corresponding Poincaré plot.

behavior in Fig. 16 is the same, while in experiment the period is always a little longer. For $\tau_R = \tau$ the oscillation is damped out; we are nearly in the case of $\tau_R \ll \tau$. Comparing our theoretical results with those in Ref. 7, which uses a partwise linear α, while we choose the realistic $\alpha(\Delta T)$ for CdS which is comparably flat, the main difference is that we lose some of the pronounced structures, and oscillations do not exist for $\tau_R = \tau$, but the general behavior remains the same.

Figure 17 shows an experimental damped oscillation in the Poincaré representation. In the beginning the structures are produced by τ_R but after a while τ is the dominating time constant, leading to a fixed point after some spiral curve. This fixed point is in the middle of the area enclosed by the oscillation loop for $\tau_R = 200$ ms, i.e., for $\tau_R \gg \tau$. This curve is also drawn in Fig. 17.

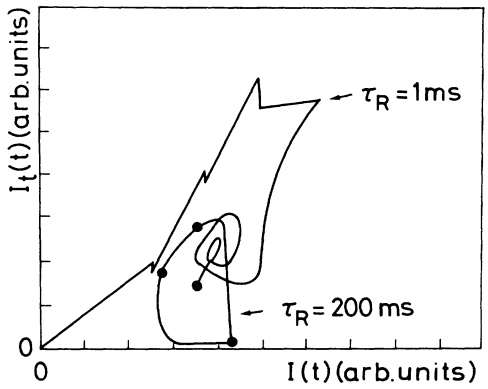

FIG. 17. Poincaré plot of a damped oscillation ($\tau_R = 1$ ms). The corresponding loop for $\tau_R = 200$ ms ($\gg \tau$) is also shown.

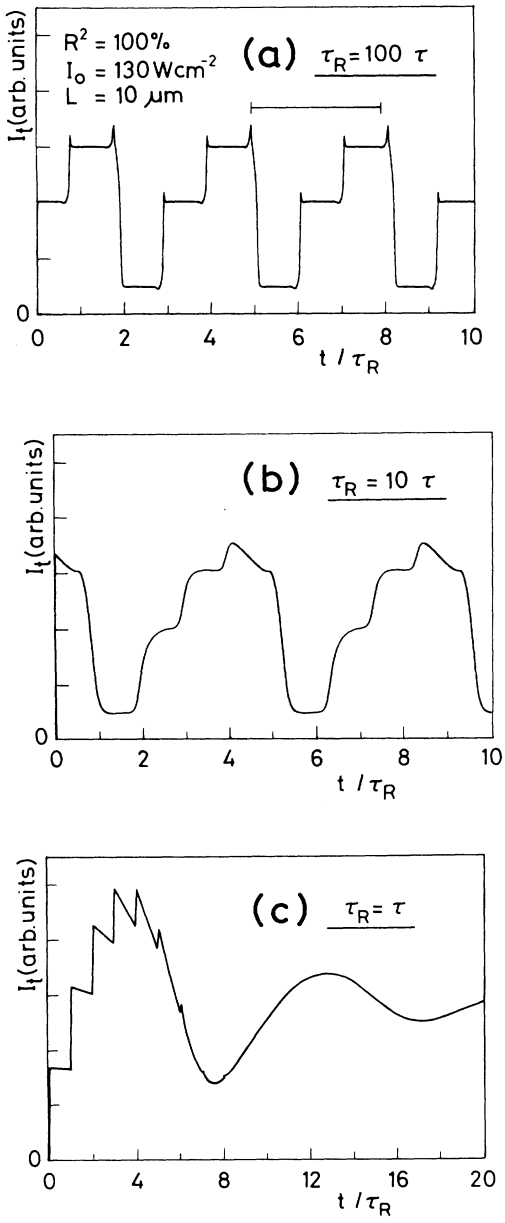

FIG. 16. Theoretical evaluation of the oscillations for decreasing τ_R at constant I_0.

To get again an overview of oscillations as a function of I_0 and τ_R, we show the same measurements as done in Fig. 14(a) but now with τ_R working as a control parameter (Fig. 18). As can be seen, oscillations are first disappearing at high I_0 when decreasing τ_R. This leads to a decrease of the oscillatory range of I_0; simultaneously the structure of the plateaus as for $\tau_R \gg \tau$ is destroyed and only modes with great T/τ_R do exist.

CONCLUSION AND OUTLOOK

We have characterized the nonlinearity of our CdS samples itself, which is under the present conditions an induced absorber leading to intrinsic OB. We investigated its own dynamic properties by measuring the critical slowing down for the first time for an induced absorber. After presenting data about the situation of an additional Fabry-Perot resonator which is related to the ring resonator in its static properties, we showed a direct way to measure the third normally unstable branch of the intrinsic (normally) bistable hysteresis of the medium. The measurements of oscillatory output from the ring cavity give experimental indications to confirm the theoretically found Farey tree structure[7(c)] of the oscillation modes as a function of the incident intensity. Only the first step of the tree is visible in the experiment, which is easily understood when looking at the theoretically expected stability of the more complicated modes.

In contrast to dispersive nonlinearities in a ring cavity, i.e., Ikeda instabilities, chaos was found neither experimentally nor theoretically for an intrinsically bistable absorber. The oscillations were found to be very stable in the limit of long round-trip times of the cavity making the all-optical system a candidate for an all-optical clock in connection with all-optical computing.

If the system is disturbed once, being in the limit $\tau_R \gg \tau$ other modes can exist also with the same system

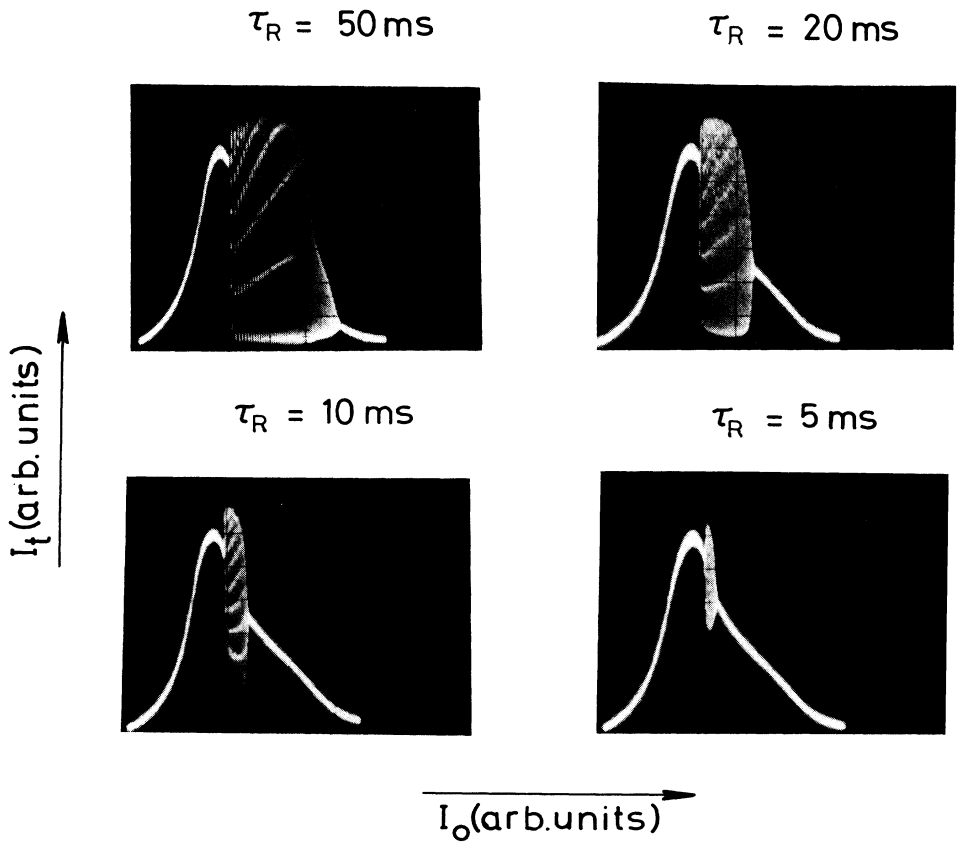

FIG. 18. Same measurement as in Fig. 14(a) but now using τ_R as the control parameter.

parameters but different initial conditions, as we shall show in a forthcoming contribution. This leads to an (in principle) infinite series of coexisting modes with higher oscillation frequencies. Once such a coexisting mode is excited, it remains stable. This effect can also be interpreted with the theoretical tools presented here. These oscillations are self-similar as a function of time.

If the induced absorber is not intrinsically bistable, as is the case for CdS in the orientation $\mathbf{E} \perp \mathbf{c}$ and $\hbar\omega = 2.410$ eV (see Ref. 6), $I_t(I_0)$ shows only a strong nonlinearity. The system shows a bifurcation route to chaos if the slope $I_t(I_0)$ is sufficiently negative. An experimental as well as theoretical discussion of this scenario will soon be published.

ACKNOWLEDGMENTS

This work is a project of the Sonderforschungsbereich 65 "Festkörperspektroskopie" financed by the Deutsche Forschungsgemeinschaft. The high quality CdS samples are grown in the Kirstall-Labor der Universität Karlsruhe and the dielectric coatings have been produced in the Institut für Quantenoptik der Universität Hannover. Stimulating discussions with Dr. M. Lindberg and Professor Dr. H. Haug (Universität Frankfurt) are acknowledged.

[1]F. Fidorra, M. Wegener, J. Y. Bigot, B. Hönerlage, and C. Klingshirn, J. Lumin. **35**, 43 (1986).

[2]C. Klingshirn, M. Wegener, C. Dörnfeld, M. Lambsdorff, J. Y. Bigot, and F. Fidorra, *Optical Bistability III,* Vol. 8 of *Springer Proceedings in Physics,* edited by H. M. Gibbs, P. Mandel, N. Peyghambarian, and S. D. Smith (Springer-Verlag, New York, 1986).

[3]M. Wegener, C. Dörnfeld, M. Lambsdorff, F. Fidorra, and C. Klingshirn, in Proceedings of the International SPIE Conference on Optical Chaos, Quebec, 1986, edited by J. Chrostowski and B. Abraham [Proc. SPIE **667**, 102 (1986)].

[4]M. Wegener and C. Klingshirn, Semiconductor Sci. Technol. (to be published).

[5]M. Dagenais and W. F. Sharfin, J. Opt. Soc. Am. B **2**, 1179 (1985).

[6]M. Lambsdorff, C. Dörnfeld, and C. Klingshirn, Z. Phys. B **64**, 403 (1986).

[7](a) M. Lindberg, S. W. Koch, and H. Haug, J. Opt. Soc. Am. B **3**, 751 (1986); (b) M. Lindberg, S. W. Koch, and H. Haug, *Optical Bistability III,* Vol. 8 of *Springer Proceedings in Physics,* edited by H. M. Gibbs, P. Mandel, N. Peyghambarian, and S. D. Smith (Springer-Verlag, New York, 1986), p. 331; (c) H.

Haug, S. W. Koch, and M. Lindberg, Phys. Scr. **34** (1986); (d) H. Haug, in Ref. 2, p. 86.

[8]K. Ikeda, H. Daido, and O. Akimoto, Phys. Rev. Lett. **45**, 709 (1980).

[9]H. M. Gibbs, F. A. Hopf, D. L. Kaplan, and R. L. Shoemaker, Phys. Rev. Lett. **46**, 474 (1981); H. Nakatsuka, S. Asaka, H. Itoh, K. Ikeda, and M. Matsuaka, *ibid.* **50**, 109 (1983), R. G. Harrison, W. J. Firth, C. A. Emshay, and I. A. Al-Saidi, *ibid.* **51**, 562 (1983).

[10]F. Urbach, Phys. Rev. **92**, 1324 (1953); W. Martienssen, J. Phys. Chem. Solids **2**, 257 (1958); for the microscopic theory of the Urbach-Martienssen rule, see, e.g., J. G. Liebler, S. Schmitt-Rink, and H. Haug, J. Lumin. **34**, 1 (1985), and the literature cited therein.

[11]D. A. B. Miller, J. Opt. Soc. Am. B **1**, 1 (1984).

[12]L. A. Lugiato, in *Progress in Optics XXI,* edited by E. Wolf (North-Holland, Amsterdam, 1984); W. Lange, F. Mitschke, R. Deserno, and J. Mlynek, Phys. Rev. A **32**, 271 (1985); J. G. H. Mathew, M. R. Taghizadek, E. Abraham, I. Janossy, and S. D. Smith, in *Optical Bistability III,* Vol. 8 of *Springer Proceedings in Physics,* edited by H. M. Gibbs, P. Mandel, N. Peyghambarian, and S. D. Smith (Springer-Verlag, New York, 1986).

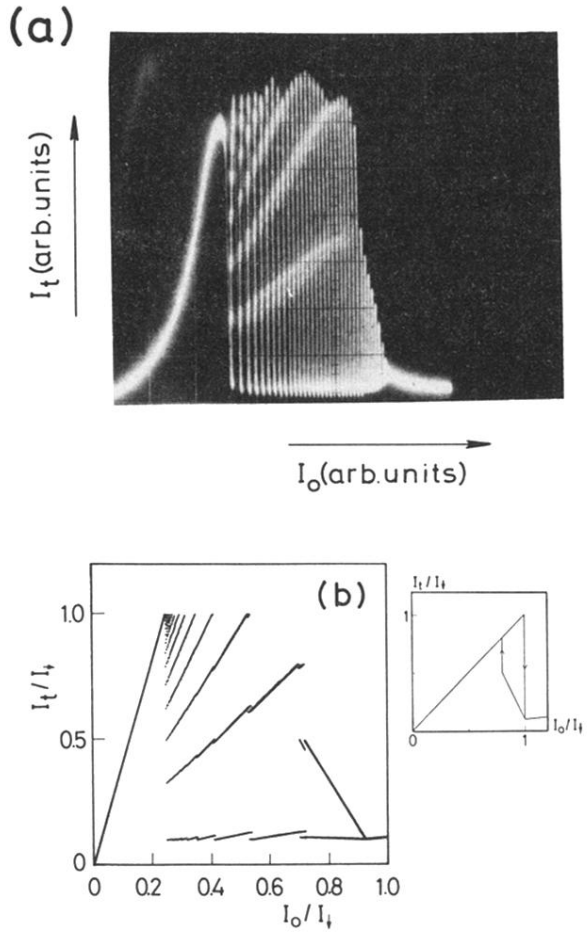

FIG. 14. (a) Experimental $I_t(I_0)$ curves using a slow ramp to increase I_0, $\tau_R = 100$ ms, $R^2 = 75\%$, $\mathbf{E}||\mathbf{C}$, $T = 300$ K, $L = 9$ μm; (b) theoretical $I_t(I_0)$ curve gained from Eq. (5) and $I_t(I)$ describing the hysteresis of a 9-μm CdS crystal as shown in the small plot.

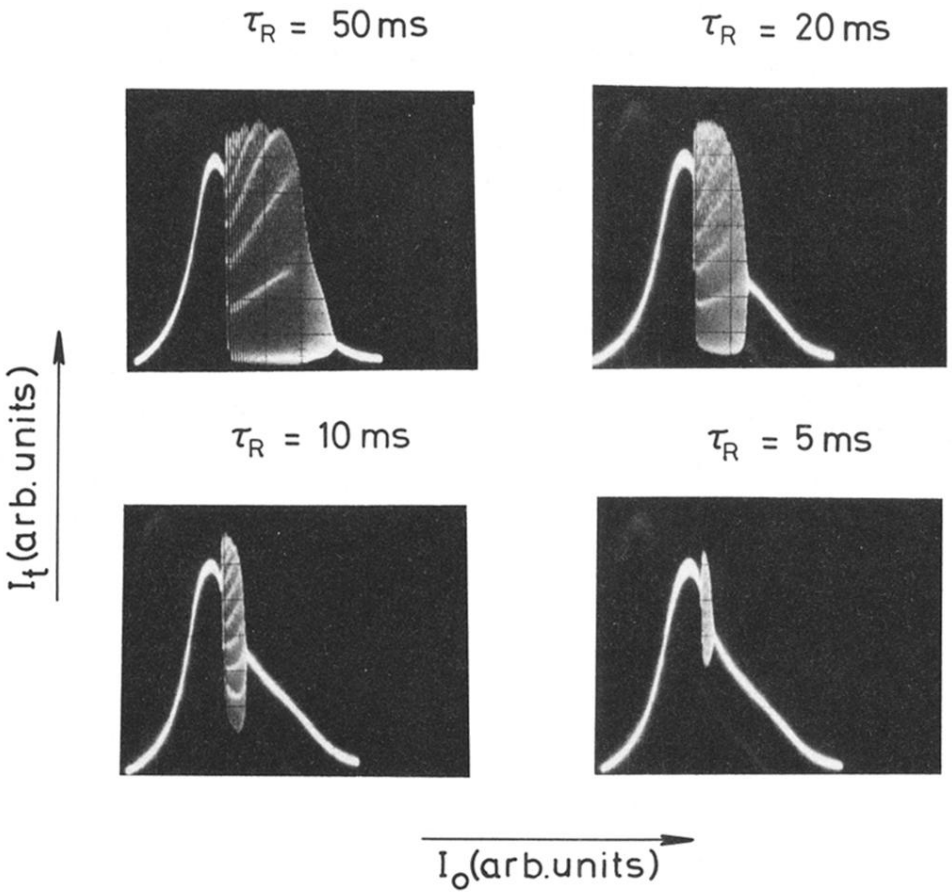

FIG. 18. Same measurement as in Fig. 14(a) but now using τ_R as the control parameter.